

A NORMED G SPACE AND WEAKENED WEAK (W^2) FORMULATION OF A CELL-BASED SMOOTHED POINT INTERPOLATION METHOD

G. R. LIU^{*,†} and G. Y. ZHANG^{†,‡}

**Centre for Advanced Computations in Engineering Science (ACES)
Department of Mechanical Engineering
National University of Singapore (NUS)
9 Engineering Drive 1, 117576, Singapore*

*†Singapore-MIT Alliance (SMA)
E4-04-10, 4 Engineering Drive 3
117576, Singapore*

‡smazg@nus.edu.sg

Received 19 December 2008

Accepted 11 January 2009

This paper presents a normed G^1 space and a weakened weak (W^2) formulation of a cell-based smoothed point interpolation method (CS-PIM) for 2D solid mechanics problems using three-node triangular cells. Displacement fields in the CS-PIM are constructed using the point interpolation method (polynomial PIM or radial PIM) and hence the shape functions possess the Kronecker delta property facilitating the easy enforcement of Dirichlet boundary conditions. The edge-based T-schemes are introduced for selecting supporting nodes for creating the PIM shape functions and an adaptive coordinate transformation (CT) technique is proposed to solve the singularity problem for the moment matrix. Smoothed strains are obtained by performing the generalized smoothing operation over each triangular background cell. Because the nodal PIM shape functions can be discontinuous, a W^2 formulation of generalized smoothed Galerkin (GS-Galerkin) weak form is then used to create the discretized system equations. Numerical examples including static, free and forced vibration problems have been studied to examine the present method in terms of accuracy, convergence, efficiency and temporal stability.

Keywords: Numerical methods; meshfree method; point interpolation method (PIM); finite element method (FEM); weakened weak form (W^2); cell-based smoothing.

1. Introduction

After more than half a century of development, finite element method (FEM) has become a very powerful and versatile technique for numerical simulation in engineering and science with many commercial software packages available

[‡]Corresponding author.

[Zienkiewicz and Taylor (2000); Liu and Quek (2003)]. A salient feature of FEM is that it divides a complicated continuum into finite number of elements, which makes the numerical treatments for complicated problems possible with the use of the Galerkin weak formulation ensuring the stability and convergence. Among types of elements used in FEM for 2D problems, the linear triangular element is the simplest one, which can always be generated efficiently and automatically without manual operation for complicated domains, and hence is preferred by the engineers. However, solutions of the linear triangular elements are generally of poor accuracy and low convergence rate, especially for stress results. The reason is that a fully compatible FEM model of assumed displacement based on the standard Galerkin weak form behaves overly-stiff.

To overcome the overly-stiff problem and to improve the performance of the fully compatible FEM results, many efforts have been made in the past, such as the development of hybrid FEM formulations [Pian and Wu (2006)]. Recently, a generalized gradient smoothing (GGS) technique for discontinuous functions, G space theory, and the notion of weakened weak (W^2) formulation have been developed by [Liu (2008a, 2008b)]. The W^2 formulation is also termed as the Generalized Smoothed Galerkin (GS-Galerkin) weak form and is the foundation of a series of novel and powerful numerical methods which can effectively solve the overly-stiff problem and hence provide very good results even using the linear triangular mesh. The GGS has been developed based on the gradient smoothing for continuous functions that has been widely used in the nonlocal continuum mechanics [Eringen and Edelen, 1972], the smoothed particle hydrodynamics (SPH) [Lucy (1977); Monaghan (1982); Liu and Liu (2003)], in solving the material instabilities [Chen Wu and Belytschko (2000)], spatial instability in nodal integrated meshfree method [Chen *et al.* (2001)], and in the development of smoothed FEM models (SFEM [Liu, Dai and Nguyen (2007); Liu and Nguyen *et al.* (2007); Dai, Liu and Nguyen (2007); Dai and Liu (2007)], NS-FEM [Liu and Nguyen *et al.* (2008)], and ES-FEM [Liu, Nguyen and Lam (2008)]). Using the GS-Galerkin weak formulation, the PIM shape and the node-based smoothing domains, a meshfree node-based smoothed point interpolation method (NS-PIM^a) has been proposed for both 2D and 3D problems [Liu and Zhang *et al.* (2005); Zhang and Liu *et al.* (2007b)]. The PIM (or radial PIM) shape functions possess the Kronecker delta property and hence facilitate the treatment of essential boundary conditions [Liu (2002)]. It was found that the NS-PIM (or NS-RPIM [Liu and Li *et al.* (2006)]) is at least linearly conforming, immune from the volumetric locking, more tolerant to mesh distortion, works well for linear triangular mesh, can provide very good stress solutions, and more importantly it can provide upper bound solutions in energy norm with respect to both FEM and exact ones [Liu and Zhang (2008a); Zhang and Liu *et al.* (2007a)]. Thus using the NS-PIM together with the FEM, we have a systematical way to numerically obtain certified

^aThe NS-PIM was originally termed as the linearly conforming point interpolation method (LC-PIM).

solutions of bounds in energy norm [Zhang, Liu and Li (2008)]. Extending the idea of NS-PIM to the FEM scheme, a node-based smoothed finite element method (NS-FEM) has been formulated for various shapes and elements [Liu and Nguyen *et al.* (2008)]. The NS-FEM can be viewed as a special case of NS-PIM using linear shape functions and possesses similar properties. However, the NS-PIM (or the NS-RPIM/NS-FEM) model is overly-soft, thus encounters the temporal instability problem for solving dynamic problems. Then by performing the gradient smoothing operation over the edge-based domains, the edge-based smoothed finite element method (ES-FEM) [Liu, Nguyen and Lam (2008); Nguyen and Liu *et al.* (2008)] and the edge-based smoothed point interpolation method (ES-PIM) [Liu and Zhang (2008b)] have been developed in the settings of FEM and meshfree methods respectively. For the ES-PIM using polynomial or radial PIM shape functions, a class of cell-based T-scheme has been proposed for selecting the supporting nodes for the approximation of field variables, i.e., T3 and T6/3 schemes for polynomial PIM shape function construction; T6 and T2L schemes for RPIM shape function construction. The cell-based T-scheme can not only solve the singularity problem but also improve the efficiency of the methods [Liu and Zhang (2008b)]. Compared with the node-based smoothing operation, the edge-based strain smoothing can properly reduce the softening effects and hence make the edge-based model have close-to-exact stiffness. Both ES-FEM and ES-PIM can provide very accurate solutions, are temporally stable and hence work well for dynamic problems.

For the numerical methods discussed previously, the smoothed strains are assumed to be constant within each smoothing domain and hence the strain fields over the problem domain are not continuous. Based on the Strain-Constructed Galerkin (SC-Galerkin) weak formulation and creating the strain fields using the linear interpolation with the smoothed strains, Liu and coworkers have developed a class of strain-constructed point interpolation methods (SC-PIM) [Liu and Zhang (2008c); Liu and Xu *et al.* (2009a, 2009b)]. The SC-PIM models can produce piecewise linear and continuous strain fields and possess a number of attractive properties including high accuracy, super convergence and upper bound solutions.

In this work, a normed G^1 space and a weakened weak (W^2) formulation for solid mechanics problems are first briefly presented. Using the W^2 formulation, a cell-based smoothed point interpolation method (CS-PIM) is developed. In the scheme of CS-PIM, displacement fields are constructed using the PIM (polynomial or radial) shape functions, the smoothed strains are obtained by performing the generalized gradient smoothing operation over each triangular background cell and the GS-Galerkin weak form is used to derive the discretized system equations. Based on the three-node triangular cells, two edge-based T-schemes (T4 and T2L schemes) of selecting nodes for creating PIM shape functions have been proposed. A general coordinate transformation (CT) technique has also been introduced to overcome the singularity problem occurred in the process of bilinear interpolation using T4 scheme. Three models of CS-PIM are developed including CS-PIM(T4-CT) using polynomial PIM shape functions and T4 scheme of CT technique to select the

supporting nodes, CS-RPIM(T4) using RPIM shape functions and T4 scheme and CS-RPIM(T2L) which uses RPIM shape functions and T2L scheme. A number of numerical examples, including static, free and forced vibration problems, will be studied to investigate the properties of the CS-PIM models.

2. Weakened Weak (W²) Formulation

2.1. Basic equations for 2D solids in strong form

Consider a two-dimensional static elasticity problem defined in domain Ω bounded by Γ ($\Gamma = \Gamma_u + \Gamma_t; \Gamma_u \cap \Gamma_t = 0$) governed by the following equations.

$$\mathbf{L}_d^T \boldsymbol{\sigma} + \mathbf{b} = 0 \quad \text{in } \Omega, \quad (1)$$

where \mathbf{L}_d is a matrix of differential operator defined as

$$\mathbf{L}_d \left(\frac{\partial}{\partial x}, \frac{\partial}{\partial y} \right) = \begin{bmatrix} \frac{\partial}{\partial x} & 0 \\ 0 & \frac{\partial}{\partial y} \\ \frac{\partial}{\partial y} & \frac{\partial}{\partial x} \end{bmatrix}. \quad (2)$$

$\boldsymbol{\sigma}^T = \{\sigma_{xx} \ \sigma_{yy} \ \tau_{xy}\}$ is the vector that collects stresses components and $\mathbf{b}^T = \{b_x \ b_y\}$ is the body force vector. The stresses relate the strains via the constitutive equation or the generalized Hook's law as follows:

$$\boldsymbol{\sigma} = \mathbf{D} \boldsymbol{\varepsilon}, \quad (3)$$

in which \mathbf{D} is the matrix of material constants that is defined as follows:

$$\mathbf{D} = \frac{E}{1-v^2} \begin{bmatrix} 1 & v & 0 \\ v & 1 & 0 \\ 0 & 0 & \frac{1-v}{2} \end{bmatrix} \quad \text{Plane stress,} \quad (4)$$

$$\mathbf{D} = \frac{E(1-v)}{(1+v)(1-2v)} \begin{bmatrix} 1 & \frac{v}{1-v} & 0 \\ \frac{v}{1-v} & 1 & 0 \\ 0 & 0 & \frac{1-2v}{2(1-v)} \end{bmatrix} \quad \text{Plane strain,}$$

where E is Young's modulus and v is Poisson's ratio.

In Eq. (3), $\boldsymbol{\varepsilon}^T = \{\varepsilon_{xx} \ \varepsilon_{yy} \ 2\varepsilon_{xy}\}$ is the vector of strains that relates to the displacements by the following compatibility equation.

$$\boldsymbol{\varepsilon} = \mathbf{L}_d \mathbf{u}, \quad (5)$$

where $\mathbf{u} = \{u_x \ u_y\}^T$ is the displacement vector. Strains obtained using Eq. (5) are generally called *compatible* strains and termed as $\tilde{\boldsymbol{\varepsilon}}$ in this work.

There are two types of boundary conditions: Dirichlet (or essential/displacement) boundary conditions and Neumann (or natural/stress) boundary conditions.

Dirichlet boundary conditions:

$$\mathbf{u} = \mathbf{u}_\Gamma \quad \text{on } \Gamma_u, \quad (6)$$

where \mathbf{u}_Γ is the vector of the prescribed displacements on the essential boundary Γ_u .

Neumann boundary conditions:

$$\mathbf{L}_n^T \boldsymbol{\sigma} = \mathbf{t}_\Gamma \quad \text{on } \Gamma_t, \quad (7)$$

where \mathbf{t}_Γ is the vector of the prescribed traction on the natural boundary Γ_t , and \mathbf{L}_n is the matrix of unit outward normal which can be expressed as

$$\mathbf{L}_n(n_x, n_y) = \begin{bmatrix} n_x & 0 \\ 0 & n_y \\ n_y & n_x \end{bmatrix}. \quad (8)$$

2.2. Definition of the normed G^1 space for functions

In constructing a normed G^1 space for functions, the problem Ω is discretized properly with a set of N_n nodes without any coinciding nodes. The problem Ω is then further tessellated properly into a set of N_s smoothing domains bounded by Γ_n^s ($n = 1, 2, \dots, N_s$) that do not share any finite portion of the line-segments where the function is discontinuous [Liu (2008a, 2008b)]. A \mathbb{G}_h^1 space can be then defined as:

$$\mathbb{G}_h^1(\Omega) = \left\{ v \mid \begin{array}{l} v(\mathbf{x}) = \sum_{n=1}^{N_n} \phi_n(\mathbf{x}) d_n = \Phi(\mathbf{x}) \mathbf{d}, \quad \mathbf{d} \in \mathbb{R}^{N_n} \\ v \in L^2(\Omega), \\ \sum_{k=1}^{N_s} \left(\int_{\Gamma_k^s} v(\xi) n_i d\xi \right)^2 > 0 \Leftrightarrow v \neq c \in \mathbb{R}; \quad i=1, \dots, d \end{array} \right. \quad (9)$$

where the subscript “ h ” indicates the space is of discrete (and hence finite) dimensions, $\mathbf{d} = \{d_1 \quad d_2 \quad \dots \quad d_{N_n}\}^T$ is the vector of nodal function values, and $\Phi(\mathbf{x})$ is the matrix of nodal shape functions of arbitrary order constructed using any PIM method discussed in the textbook [Liu (2002)] and can be written as

$$\Phi(\mathbf{x}) = [\varphi_1(\mathbf{x}) \quad \varphi_2(\mathbf{x}) \quad \dots \quad \varphi_{N_n}(\mathbf{x})]. \quad (10)$$

In creating functions in \mathbb{G}_h^1 spaces, we require the following conditions:

- (1) *Linearly independency condition*: all these nodal shape functions are linearly independent over Ω and hence are capable to form a basis.
- (2) *Bound condition*: all the functions constructed using these shape function must be square integrable over the problems domain. This is to ensure the convergence of the discrete model to be created.

(3) *Positivity conditions:* there exist a division of smoothing domains such that

$$\sum_{k=1}^{N_s} \left(\int_{\Gamma_k^i} \mathbf{v}(\boldsymbol{\xi}) n_i d\boldsymbol{\xi} \right)^2 > 0 \Leftrightarrow \mathbf{v} = \mathbf{c} \in \mathbb{R}, \forall \mathbf{d} \in \mathbb{R}^{N_n} \text{ and } i = 1, \dots, d. \text{ This (together with the linearly independent condition) ensures the stability of the model.}$$

When PIM or RPIM shape functions [Liu (2002)] are used, the functions constructed will in general not be continuous over the entire problem domain and hence are not compatible. Such an interpolant is not in a \mathbb{H}_h^1 space, but in a \mathbb{G}_h^1 space, because all these three conditions can be satisfied, as shown in [Liu (2008b)].

The major difference between a \mathbb{G}_h^1 space and \mathbb{H}_h^1 space is that the \mathbb{H}_h^1 space requires the first gradient of the function square integrable, but in the \mathbb{G}_h^1 space only the function itself needs to be square integrable. Therefore, the requirement on function is now further weakened upon the already weakened requirement for functions in an \mathbb{H}_h^1 space: a weakened weak requirement. Therefore, a \mathbb{G}_h^1 space can be viewed as a space of functions with weakened weak (W^2) requirements on continuity. In an \mathbb{H}_h^1 space, the bound condition is achieved by imposing the smoothness upon the first derivatives of the function being square integrable, while in the \mathbb{G}_h^1 space, it is controlled by imposing the smoothness only on the function being square integrable and with a properly constructed smoothing domains. The stability is automatically ensured for functions in an \mathbb{H}_h^1 space as long as the smoothness is satisfied, due to the Poincare-Friedrichs inequality. The stability in the \mathbb{G}_h^1 space, however, is ensured by imposing the above-mentioned positivity condition.

We note that any function created using a set of shape functions that satisfy the above-mentioned three conditions is also in the \mathbb{G}_h^1 space. A \mathbb{G}_h^1 space is indeed very accommodating and inclusive, and hence shall have much wider applications. Because a member in a \mathbb{G}_h^1 space is also a member of the \mathbb{L}_2 (Lebesgue) space, therefore a \mathbb{G}_h^1 space is a subspace of \mathbb{L}_2 space: $\mathbb{G}_h^1(\Omega) \subset \mathbb{L}^2(\Omega)$.

We finally define a space of functions that is fixed on the homogenous Dirichlet boundaries and hence the functions cannot “float”.

$$\mathbb{G}_{h,0}^1 = \{ \mathbf{v} \in \mathbb{G}_h^1(\Omega) | \mathbf{v} = 0 \text{ on } \Gamma_u \}. \quad (11)$$

2.3. A weakened weak (W^2) form statement: GS-Galerkin

For solid mechanics problems given in the strong statements in Sec. 2.1, our W^2 statement becomes: an approximated solution $\bar{\mathbf{u}} \in \mathbb{G}_{h,0}^1$ associated with the strong statements in Sec. 2.1 satisfies

$$\bar{a}_D(\bar{\mathbf{u}}, \mathbf{v}) = f(\mathbf{v}), \quad \forall \mathbf{v} \in \mathbb{G}_{h,0}^1, \quad (12)$$

where

$$\bar{a}_D(\mathbf{u}, \mathbf{v}) = \sum_{i=1}^{N_s} A_i^s \bar{\boldsymbol{\xi}}_i^T(\mathbf{u}) \mathbf{D} \bar{\boldsymbol{\xi}}_i(\mathbf{v}), \quad \mathbf{u}, \mathbf{v} \in \mathbb{G}_h^1 \quad (13)$$

where A_i^s is the area of the i th smoothing domain, $\bar{\boldsymbol{\varepsilon}}_i$ is the vector of the generalized smoothed strains in the smoothed domain. For *any* given vector field of displacement $\mathbf{u} = \{u_1 \ u_2\}^T$ with two components $u_1, u_2 \in \mathbb{G}_h^1$, $\bar{\boldsymbol{\varepsilon}}_i$ can be written as [Liu (2008a)]:

$$\bar{\boldsymbol{\varepsilon}}_i(\mathbf{u}) = \frac{1}{A_i^s} \int_{\Gamma_i^s} \mathbf{L}_n \mathbf{u}(\mathbf{x}) ds = \{\bar{\varepsilon}_{xx} \ \bar{\varepsilon}_{yy} \ 2\bar{\varepsilon}_{xy}\}_i^T, \quad (14)$$

which is in fact a boundary flux approximated strain.

In Eq. (12), the *linear functional* for the solid mechanics problem is defined as

$$f(\mathbf{v}) = \int_{\Gamma_t} \mathbf{v}^T \mathbf{t}_\Gamma d\Omega + \int_{\Omega} \mathbf{v}^T \mathbf{b} d\Omega, \quad \mathbf{v} \in \mathbb{G}_h^1. \quad (15)$$

The important properties of the generalized smoothed bi-linear form \bar{a}_D and the stability, convergence of the W^2 formulation defined in Eq. (12) can be found in [Liu (2008a, 2008b)].

3. Formulation for the Cell-Based Smoothed Point Interpolation (CS-PIM)

3.1. Displacement approximation using PIM

For the numerical models developed in this work, the assumed displacement fields are constructed locally using the point interpolation method (PIM) with a small set of supporting nodes at the point of interest. There are two types of PIM shape functions that have been developed using different basis functions, i.e. polynomial PIM using polynomial basis functions [Liu and Gu (2001)] and radial PIM (RPIM) using radial basis functions [Wang and Liu (2002)]. Details of how to construct PIM shape functions can be found in the meshfree books [Liu (2002); Liu and Gu (2005)], and we only give a brief introduction here.

For the approximation using polynomial PIM, the formulations start with the following assumption:

$$u(\mathbf{x}) = \sum_{i=1}^n P_i(\mathbf{x}) a_i = \mathbf{P}^T(\mathbf{x}) \mathbf{a}, \quad (16)$$

where $u(\mathbf{x})$ is a field variable function defined in the Cartesian coordinate space $\mathbf{x}^T = \{x \ y\}$, $P_i(\mathbf{x})$ is the basis function of monomials which is usually built utilizing the Pascal's triangles, a_i is the corresponding coefficient, and n is the number of nodes in the local support domain. The complete polynomial basis of orders 1 and 2 can be written as

$$\begin{aligned} \mathbf{P}^T(\mathbf{x}) &= \{1 \ x \ y\} && \text{Basis of complete 1st order} \\ \mathbf{P}^T(\mathbf{x}) &= \{1 \ x \ y \ x^2 \ xy \ y^2\} && \text{Basis of complete 2nd order} \end{aligned} \quad (17)$$

For the approximation using radial PIM, the field function can be approximated by radial basis functions augmented with polynomials as follows:

$$u(\mathbf{x}) = \sum_{i=1}^n R_i(\mathbf{x}) a_i + \sum_{j=1}^m P_j(\mathbf{x}) b_j = \mathbf{R}^T(\mathbf{x}) \mathbf{a} + \mathbf{P}^T(\mathbf{x}) \mathbf{b}, \quad (18)$$

where $R_i(\mathbf{x})$ and $P_j(\mathbf{x})$ are radial basis functions and polynomial basis functions respectively, a_i and b_i are corresponding coefficients, n is the number of nodes in the local support domain and m is the number of polynomial terms.

The coefficients in Eqs. (16) and (18) can be determined by enforcing the field function to be satisfied at the n nodes within the local support domain. Finally, the PIM shape functions can be obtained and the field function can be expressed as

$$u(\mathbf{x}) = \sum_{i=1}^n \varphi_i(\mathbf{x})d_i = \Phi^T(\mathbf{x})\mathbf{d}, \quad (19)$$

where d_i is a nodal function value and $\varphi_i(\mathbf{x})$ is the PIM shape function (polynomial PIM or radial PIM) which possesses the Kronecker delta property.

3.2. Edge based T-schemes for nodes selection

The PIM shape functions in Eq. (19) are obtained under the assumption that the moment matrix is invertible. The RPIM shape functions can always be constructed because the radial moment matrix is always invertible for arbitrary scattered nodes as long as to avoid using some specific shape parameters [Powell (1992)]. However, for the construction of polynomial PIM shape functions, some measures are needed to ensure the existence of the inverse matrix. In the previous work, a number of methods for handling the singular moment matrix can be found in [Liu (2002)]. Recently, a set of node selection schemes, cell-based T-schemes, have been presented and work well in the schemes of NS-PIM and ES-PIM models [Liu and Zhang *et al.* (2005); Liu and Zhang (2008b)].

The schemes for node selections can be performed based on a set of background triangular cells to ensure quality patterns of supporting points and efficiency in computing PIM shape functions. Depending on the location of the point of interest (that is usually the quadrature point), the node selection schemes are different. In our W^2 formulations based on G^1 space theory, the points of interests are on the boundary of the smoothing domain Γ^s . In the NS-PIM and ES-PIM, most quadrature points are located within the triangular background cells, then the T-schemes for node selection are associated with the triangular cells and hence they are called cell-based T-schemes. Note that to ensure the exact enforcement of linear boundary conditions and hence the linear conformability of the model, cell-based T-schemes use only linear interpolation for the point of interest located on the problem boundaries. For the present CS-PIM models, on the other hand, the smoothing domains are the same as the triangular cells and hence the point of interest or the the quadrature points are located on the edges of the triangular cells. Hence we need to select nodes for the interpolation for the quadrature points on the edges of background triangles, which is called edge-based T-schemes of node selection. The following details these T-schemes.

In the following definition of edge-based T-schemes, edges of the triangles are classified into two groups: interior edges and boundary edges. If the edge is located inside the problem domain, this edge is then called an interior edge. Correspondingly, if the edge is on the problem boundaries, then we call it a boundary edge.

Edge-based T2 scheme

The edge-based T2 scheme simply selects the two end-nodes of an edge of a cell. In this simple case, piecewisely linear displacement field is used, the compatible strain in the cell is constant, the smoothing operation has no effect, and the CS-PIM model created will be exactly the same as the FEM(T3) model. Therefore, this scheme will not be discussed further and will be simply referred as FEM(T3) model in this work.

Edge-based T4 scheme

The edge-based T4 scheme selects four nodes for the interpolation for a point located on an interior edge and two nodes for those located on boundary edges. As illustrated in (a) of Fig. 1, when the point of interest (\mathbf{x}) located on an interior edge (i), four nodes ($i_1 - i_4$) are selected which are the vertexes of the two neighboring cells of edge i . When (\mathbf{x}) located on a boundary edge (j), as shown in (b) of Fig. 1, only two nodes ($j_1 - j_2$) are used which are the end-points of edge j .

The edge-based T4 scheme can be used to select nodes for the construction of both polynomial PIM and RPIM shape functions. As we mentioned previously, the RPIM shape functions can always be obtained using arbitrary scattered nodes as long as some specific shape parameters are not used. When 4 (or more) arbitrarily distributed nodes are used to construct PIM shape functions, the moment matrix can be singular and a number of methods have been suggested in [Liu (2002)] to overcome the singularity problem, including the coordinate transformation technique. In this work, we proposed the following adaptive coordinate transformation (CT) technique that works particularly well for 4-node interpolation.

Consider now that 4 nodes have been selected for PIM shape function construction. We then use 4 terms of polynomial basis functions of lowest order, which leads to a set of bilinear PIM shape functions. The bilinear PIM shape functions at a point $\mathbf{x}_e = [x_e \ y_e]^T$ can be finally expressed as follows.

$$\varphi(\mathbf{x}_e) = [1 \ x_e \ y_e \ x_e y_e] \underbrace{\begin{bmatrix} 1 & x_1 & y_1 & x_1 y_1 \\ 1 & x_2 & y_2 & x_2 y_2 \\ 1 & x_3 & y_3 & x_3 y_3 \\ 1 & x_4 & y_4 & x_4 y_4 \end{bmatrix}}_{\mathbf{P}_n}^{-1}, \quad (20)$$

where $\mathbf{x}_i = [x_i \ y_i]^T (i = 1, 2, 3, 4)$ are the coordinates of the four nodes selected using the T4 scheme. It is well-known the inverse of the moment matrix (\mathbf{P}_n) may

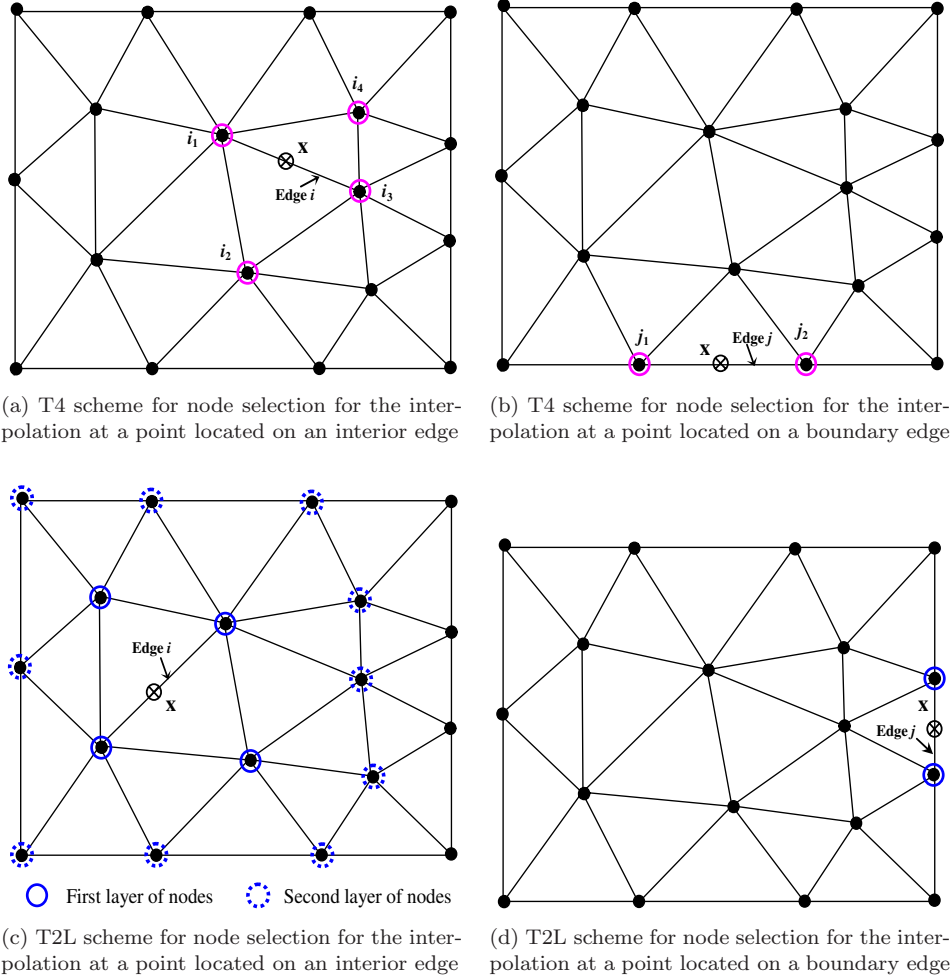


Fig. 1. Illustration of edge-based T-schemes for supporting nodes selection based on three-node triangular cells for constructing PIM shape functions for the interpolation at a point located on an edge.

not exist, or the matrix may be ill-conditioned as discussed in the book [Liu (2002)]. In these cases, we apply the following coordinate transformation technique.

$$\begin{cases} \xi = (x - x_e) \cos \gamma + (y - y_e) \sin \gamma \\ \eta = -(x - x_e) \sin \gamma + (y - y_e) \cos \gamma \end{cases} \quad (21)$$

where (x_e, y_e) is the origin of the local coordinates system (ξ, η) , which is defined in the global coordinate system (x, y) , and (γ) is the rotation angle between the local and global coordinates system.

Applying Eq. (21) to the four supporting nodes and the point of interest, the bilinear PIM shape functions in Eq. (20) becomes

$$\varphi(\mathbf{x}_e) = [1 \quad 0 \quad 0 \quad 0] \underbrace{\begin{bmatrix} 1 & \xi_1 & \eta_1 & \xi_1\eta_1 \\ 1 & \xi_2 & \eta_2 & \xi_2\eta_2 \\ 1 & \xi_3 & \eta_3 & \xi_3\eta_3 \\ 1 & \xi_4 & \eta_4 & \xi_4\eta_4 \end{bmatrix}^{-1}}_{\mathbf{P}'_n} \quad (22)$$

Using the above transformation with a proper γ , the singularity problem of the polynomial moment matrix can be solved and shape functions at $\mathbf{x}_e = [x_e \quad y_e]^T$ can finally be obtained. However, there are two issues need to be addressed: a proper indicator which can tell us when to perform the coordinate transform on the object matrix (\mathbf{P}_n) and a proper (γ) which should make the new matrix (\mathbf{P}'_n) well-conditioned.

In this study, the determinant of the moment matrix is used as the indicator, for which we use a square cell as a base cell. Figure 2(a) shows four nodes located at the vertexes of a square cell with edge length ($2a$) in the coordinates system (x, y). If we used these four nodes to create the bilinear interpolation at a point located inside the square, a moment matrix \mathbf{P}_n in Eq. (20) can be obtained. Rotating the square around the origin, different moment matrixes can be obtained using the new set of coordinates of the four vertexes. The determinant of the moment matrix (d) can

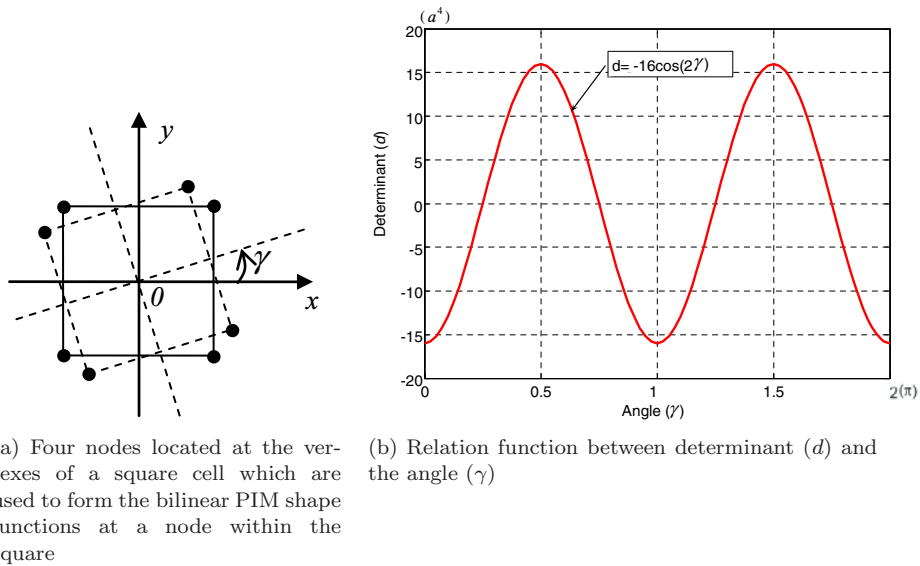


Fig. 2. Coordinate transformation (CT) technique for overcoming the singular moment matrix. Relation between the rotation angle and the determinate of the moment matrix using the four vertexes of a square cell with edges of $2a$.

then be computed and it should relate to the transformation angle (γ), as shown in (b) of Fig. 2. It turns out the relation has the following simple form.

$$d = -16a^4 \cos(2\gamma) \quad (23)$$

Based on the above relationship function for the base cell, we proposed the following adaptive coordinate transformation (CT) technique for creating bilinear PIM shape functions.

- (1) Using the T4 scheme, determine the four supporting nodes for the interpolation for a point located on an interior edge of length L , and calculate the determinant of the moment matrix (d_1) using these four nodes.
- (2) Calculate the determinant of a matrix (d_0) for the base square cell with length L .
- (3) If ($|d_1| < |d_0|$), we perform the following coordinate transformation.
 - (i) Letting $d = d_1$ in Eq. (23), we can obtain a value of the angle (γ_1) which satisfies ($\gamma_1 \leq \pi/2$).
 - (ii) Substituting ($\pm\gamma_1$) into Eq. (21) and calculate determinates of the two new matrixes as shown in Eq. (22).
 - (iii) Select the angle from ($\pm\gamma_1$) which gives a bigger value of determinant, use it to perform the coordinate transformation and finally obtain the shape functions using Eq. (22).

The above CT technique is simple can effectively resolve the singularity problem in an adaptive manner according to the current trade distribution, and hence ensures the creating of the quality bilinear PIM shape functions as long as these four nodes are not in-line.

Edge-based T2L scheme

The edge-based T2L scheme selects two layers of nodes for the interpolation at a point located on interior edges. As shown in (c) of Fig. 1, the first layer of nodes are exactly those selected using the edge-based T4 scheme, and the second layer contains those nodes which are directly connected to the nodes of first layer. As we discussed previously, the T2L scheme selects two nodes to perform the linear interpolation for those points located on boundary edges, as shown in (d) of Fig. 1.

The T2L scheme is used to select supporting nodes for constructing the RPIM shape functions, which usually uses much more nodes than the T4 scheme does and hence is more time consuming. We can use this scheme to create RPIM shape functions with high order of consistence and for extremely irregularly distributed nodes.

The nodal PIM shape functions constructed using the above mentioned schemes will be linearly independent as long as the moment matrix is not singular [Liu (2002)], squarely integrable over the problems domain, and hence the first two conditions listed below Eq. (10) will be satisfied. Therefore, they can be used to construct functions in a \mathbb{G}_h^1 space for our W^2 formulation.

3.3. Cell-based smoothed strains

In a W^2 formulation, the smoothed strains are obtained using the generalized smoothing operation Eq. (14) with displacement fields constructed using PIM shape functions that may be discontinuous [Liu (2008a, 2008b)]. The smoothing domains are generally constructed based on the triangular background cells and the basic rule is we do not allow the boundary of smoothing domains share any finite parts of the discontinuous line segments for the assumed displacement field. In the scheme of present CS-PIM, the triangular background cells will be used to serve as smoothing domains and also the integrations cells, as shown in Fig. 3. Because our PIM shape functions are created for points on the edges of the cells, they are always continuous there. The discontinuous line segments of PIM shape functions will be inside the cell. Hence, the basic rule is well observed in our CS-PIM settings.

Note also that in a CS-PIM model, the numbers of the smoothing domains (N_s) and quadrature (integration) cells (N_Q) equal the number of triangular cells (N_e) : $N_s = N_Q = N_e$. Such a set of cell-based smoothing domains are linearly independent and satisfies the condition of minimum number of smoothing domains [Liu (2008a)]. Thus, the 3rd conditions listed below Eq. (10) are satisfied. Therefore, the generalized smoothed bi-linear form \bar{a}_D will have all these important properties given in [Liu (2008a, b)], and our W^2 formulation will be stable, converge to the exact solution, which will be shown in the example section.

Performing the generalized gradient smoothing operation within each triangular background cell and substituting Equation (19) into Equation (14), the cell-based smoothed strain, $\bar{\epsilon}_k$, can now be written in the following matrix form of nodal displacements.

$$\bar{\epsilon}_k = \frac{1}{A_k^s} \int_{\Gamma_k^s} \mathbf{L}_n \Phi \mathbf{d}_i d\Gamma = \sum_{i \in N_{inft}} \bar{\mathbf{B}}_i(\mathbf{x}_k) \mathbf{d}_i, \quad (24)$$

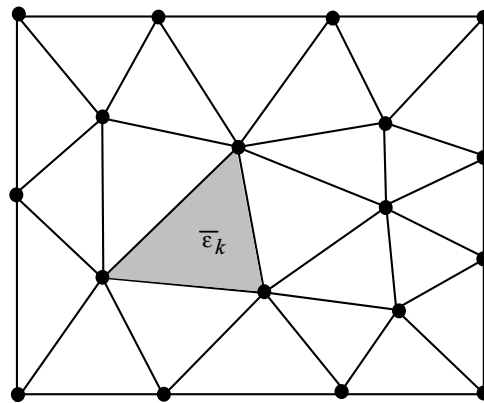


Fig. 3. Illustration of cell-based smoothing domains, which are exactly the triangular background cells and also serve as integration cells.

where Φ is the matrix of PIM shape functions, N_{infl} is the number of field nodes involved in constructing the smoothed strain fields within the cell-based smoothing domain Ω_k^s , and $\bar{\mathbf{B}}_i(\mathbf{x}_k)$ is termed as the *smoothed* strain matrix that can be expressed as

$$\bar{\mathbf{B}}_i(\mathbf{x}_k) = \begin{bmatrix} \bar{b}_{ix}(\mathbf{x}_k) & 0 \\ 0 & \bar{b}_{iy}(\mathbf{x}_k) \\ \bar{b}_{iy}(\mathbf{x}_k) & \bar{b}_{ix}(\mathbf{x}_k) \end{bmatrix}. \quad (25)$$

In the above equation, elements of the smoothed strain matrix are obtained as

$$\bar{b}_{il}(\mathbf{x}_k) = \frac{1}{A_k^s} \int_{\Gamma_k^s} \varphi_i(\mathbf{x}_k) n_l(\mathbf{x}_k) d\Gamma \quad (l = x, y). \quad (26)$$

Using Gauss integration scheme, the above integration can be further expressed as follows.

$$\bar{b}_{il} = \frac{1}{A_k^s} \sum_{m=1}^{N_{seg}} \left[\sum_{n=1}^{N_{gau}} w_n \varphi_i(\mathbf{x}_{mn}) n_l(\mathbf{x}_m) \right] \quad (l = x, y) \quad (27)$$

where N_{seg} is the number of segments of the boundary Γ_k^5 which is 3 for the CS-PIM using triangular cells, N_{gau} is the number of Gauss points located in each segment on Γ_k^s , and w_n is the corresponding weight number of Gauss integration scheme. In the present method, as bilinear or RPIM shape functions are used, $N_{gau} = 2$ is adopted in Eq. (27).

3.4. Discretized system equations

The displacement field of the present method is not continuous, thus the following generalized smoothed Galerkin (GS-Galerkin) weak form, given in Eq. (12) [Liu (2008a, 2008b)], is used to derive the discretized system equations.

Consider a deformable body occupying domain Ω in motion, subjected to body forces \mathbf{b} , external applied traction \mathbf{t}_Γ on boundary Γ_t and displacement boundary conditions $\mathbf{u} = \bar{\mathbf{u}}$ on Γ_u . If the inertial and damping forces are also considered in the dynamic equilibrium equations, the GS-Galerkin weak formulation can be presented as

$$\int_{\Omega} \delta(\bar{\boldsymbol{\varepsilon}}(\mathbf{u}))^T \mathbf{D}(\bar{\boldsymbol{\varepsilon}}(\mathbf{u})) d\Omega - \int_{\Omega} \delta \mathbf{u}^T [\mathbf{b} - \rho \ddot{\mathbf{u}} - c \dot{\mathbf{u}}] d\Omega - \int_{\Gamma_t} \delta \mathbf{u}^T \mathbf{t}_\Gamma d\Gamma = 0 \quad (28)$$

It can be found that the above GS-Galerkin weak form has the same form as the standard Galerkin weakform. Thus the formulation procedure is exactly as same as that in the standard FEM and all we need to do is to use the cell-based smoothed strain $\bar{\boldsymbol{\varepsilon}}$ in place of the compatible strain $\boldsymbol{\varepsilon}$. The overall procedure of the CS-PIM models is as follows: (1) constructing the displacement field by using PIM and the supporting nodes selected by edge-based T4 or T2L schemes, (2) obtaining the cell-based smoothed strains $\bar{\boldsymbol{\varepsilon}}$ using Eq. (24), (3) substituting the

assumed displacements and the smoothed strains into the GS-Galerkin weak form (Eq. (28)), and invoking the arbitrary nature of the variation operations, a set of discretized algebraic system equation can be obtained in the following matrix form.

$$\mathbf{M}\ddot{\mathbf{d}} + \mathbf{C}\dot{\mathbf{d}} + \bar{\mathbf{K}}\mathbf{d} = \mathbf{f}, \quad (29)$$

where \mathbf{M} is the mass matrix, \mathbf{C} is the damping matrix and \mathbf{f} is the force vector which are defined as

$$\mathbf{M} = \int_{\Omega} \rho \Phi^T \Phi d\Omega, \quad (30)$$

$$\mathbf{C} = \int_{\Omega} c \Phi^T \Phi d\Omega, \quad (31)$$

$$\mathbf{f} = - \int_{\Omega} \Phi^T \mathbf{b} d\Omega + \int_{\Gamma_t} \Phi^T \mathbf{t}_{\Gamma} d\Gamma, \quad (32)$$

in which ρ is the mass density and c is the damping parameter.

In Eq. (29), the stiffness matrix $\bar{\mathbf{K}}$ is assembled from the sub-stiffness matrix for all the integration cells, which are exactly the cell-based smoothing domains for the present method.

$$\bar{\mathbf{K}}_{ij} = \sum_{k=1}^{N_Q} A_k^s \bar{\mathbf{B}}_i^T \mathbf{D} \bar{\mathbf{B}}_j = \sum_{k=1}^{N_e} A_k^s \bar{\mathbf{B}}_i^T \mathbf{D} \bar{\mathbf{B}}_j, \quad (33)$$

where the smoothed strain matrixes are obtained using Eq. (25).

3.5. Static, free and forced vibration analysis

For static problems, the equation can be obtained imply by removing the dynamic terms in Eq. (29):

$$\bar{\mathbf{K}}\mathbf{d} = \mathbf{f}. \quad (34)$$

For free vibration analysis, we do not consider the damping and the force terms, and hence Eq. (29) reduces to

$$\mathbf{M}\ddot{\mathbf{d}} + \bar{\mathbf{K}}\mathbf{d} = \mathbf{0}. \quad (35)$$

A general solution of such an equation can be written as

$$\mathbf{d} = \mathbf{d}_A \exp(i\omega t), \quad (36)$$

where t indicates time, \mathbf{d}_A is the amplitude of the nodal displacement or the eigenvector and ω is natural frequency that is found from

$$(-\omega^2 \mathbf{M} + \bar{\mathbf{K}})\mathbf{d}_A = \mathbf{0}. \quad (37)$$

For forced vibration analysis, Equation (29) can be solved by direct integration methods in the same way as in the FEM. For simplicity, the Rayleigh damping is

considered in this study, and damping matrix \mathbf{C} is assumed to be a linear combination of \mathbf{M} and $\bar{\mathbf{K}}$,

$$\mathbf{C} = \alpha\mathbf{M} + \beta\bar{\mathbf{K}}, \quad (38)$$

where α and β are the Rayleigh damping coefficients.

Many direct integration schemes can be used to solve the second-order time dependent problems, such as the Newmark method, Grank-Nicholson method, etc. In this work, we use the Newmark method to solve the forced vibration problems. When the state at $t = t_0(\mathbf{d}_0, \dot{\mathbf{d}}_0, \ddot{\mathbf{d}}_0)$ is known, we aim to find the new state at $t_1 = t_0 + \theta\Delta t(\mathbf{d}_1, \dot{\mathbf{d}}_1, \ddot{\mathbf{d}}_1)$ where $0.5 \leq \theta \leq 1$, using the following formulations:

$$\begin{aligned} \left[\left(\alpha + \frac{1}{\theta\Delta t} \right) \mathbf{M} + (\beta + \theta\Delta t)\bar{\mathbf{K}} \right] \mathbf{d}_1 &= \theta\Delta t\mathbf{f}_1 + (1 - \theta)\Delta t\mathbf{f}_0 + \left(\alpha + \frac{1}{\theta\Delta t} \right) \mathbf{M}\mathbf{d}_0 \\ &+ \frac{1}{\theta}\mathbf{M}\dot{\mathbf{d}}_0 + [\beta - (1 - \theta)]\bar{\mathbf{K}}\mathbf{d}_0, \end{aligned} \quad (39)$$

$$\dot{\mathbf{d}}_1 = \frac{1}{\theta\Delta t}(\mathbf{d}_1 - \mathbf{d}_0) - \frac{1 - \theta}{\theta}\dot{\mathbf{d}}_0, \quad (40)$$

$$\ddot{\mathbf{d}}_1 = \frac{1}{\theta\Delta t}(\dot{\mathbf{d}}_1 - \dot{\mathbf{d}}_0) - \frac{1 - \theta}{\theta}\ddot{\mathbf{d}}_0. \quad (41)$$

4. Numerical Implementation

4.1. CS-PIM models

For all the models of CS-PIM, cell-based smoothed strains are used. The smoothed strains are obtained using the generalized stain smoothing operation within each triangular background cells. Based on the different types of PIM shape functions used (polynomial PIM or radial PIM) and different T-schemes (edge-based T4 or T2L schemes) adopted for selecting nodes, the following CS-PIM models have been created.

CS-PIM(T2)

This is the simplest CS-PIM model and is exactly the same as the FEM(T3), and hence is a fully compatible model. The CS-PIM(T2) is therefore referred as FEM(T3) in this work.

CS-PIM(T4-CT)

In the frame of CS-PIM(T4-CT), the displacement field is constructed using polynomial PIM shape functions and supporting nodes selected by the edge-based T4 scheme with the CT technique. In this case we have bilinear displacement fields within the problem domain and linear displacements along the problem boundaries. The displacement field of the CS-PIM(T4-CT) is incompatible.

CS-RPIM(T4)

The displacement field in the scheme of the CS-RPIM(T4) is constructed using radial PIM shape functions and supporting nodes selected by the edge-based T4 scheme without CT technique. The displacement field of the CS-RPIM(T4) is incompatible.

CS-RPIM(T2L)

In the CS-RPIM(T2L), we construct the displacement fields using radial PIM shape functions and supporting nodes selected by the edge-based T2L scheme. Compared to the above two models, the CS-RPIM(T2L) will use much more nodes for the interpolation and hence is more computationally expensive. The displacement field in the CS-PIM(T2L) model is incompatible.

4.2. Standard patch test

We examine the conformability property of the present method using the following standard (linear) patch test. Satisfaction of standard patch test requires that the displacements of all the interior nodes inside the patch follow “exactly” (to machine precision) the same linear function of the imposed displacement on the boundary of the patch. Therefore, passing the standard patch test can numerically ensure a numerical method convergence to the exact solution [Zienkiewicz and Taylor (2000)].

A square patch discretized using 214 irregularly distributed nodes, as shown in Fig. 4, is studied using the present methods. The following linear displacements are prescribed on all the boundaries.

$$\begin{cases} u_x = 0.6x \\ u_y = 0.6y \end{cases} . \quad (42)$$

The analytical solution for this patch test is a linear displacement field given by the above equation over the entire patch. The following error norm in displacements is used to examine the computed results.

$$e_d = \sqrt{\frac{\sum_{i=1}^{N_n} (u_i^{exact} - u_i^{nume})^2}{\sum_{i=1}^{N_n} (u_i^{exact})^2}} , \quad (43)$$

where the superscript *exact* denotes the exact or analytical solution, *nume* denotes a numerical solution obtained using a numerical method including the present CS-PIM and N_n is the number of total field nodes.

Table 1 lists the displacement norm errors of numerical results for the standard patch test obtained using the three models of CS-PIM. We found that all the CS-PIM models can pass the patch test to machine accuracy and hence are capable

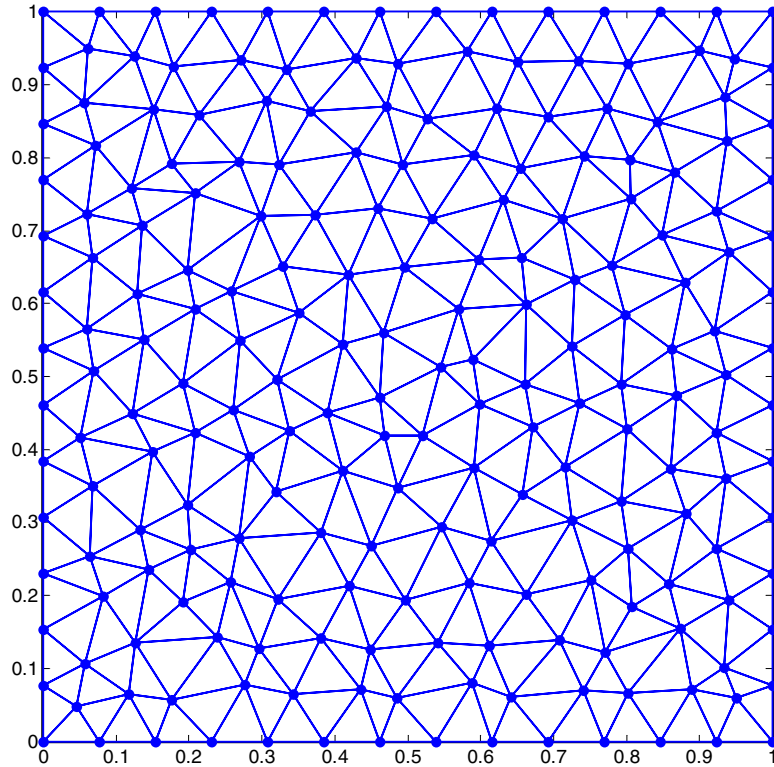


Fig. 4. Patch of unique square discretized with 214 irregularly distributed nodes.

Table 1. Error norm in displacements of numerical results for the standard patch obtained using CS-PIMs.

CS-PIM models	Error in displacement norm
CS-PIM(T4-CT)	4.3209606E-15
CS-RPIM(T4)	1.2270583E-14
CS-RPIM(T2L)	1.4090296E-15

to reproduce linear displacement fields “exactly”. This confirms numerically our theory of W^2 formulation. Note that to exactly impose the linear Dirichlet boundary conditions along the problem boundaries, linear interpolation has been used for the points of interest located on the boundaries, which has been introduced in the definition of the edge-based T-schemes.

5. Numerical Examples

Some benchmark numerical examples, including static, free and forced vibration problems, are studied in this section. Except the displacement error norm defined

in Eq. (43), the following energy error norm is also defined as follows for the later study.

$$e_e = \frac{1}{A} \sqrt{\frac{1}{2} \int_{\Omega} (\boldsymbol{\varepsilon}^{exact} - \boldsymbol{\varepsilon}^{nume})^T \mathbf{D} (\boldsymbol{\varepsilon}^{exact} - \boldsymbol{\varepsilon}^{nume}) d\Omega}, \quad (44)$$

where $\boldsymbol{\varepsilon}^{exact}$ and $\boldsymbol{\varepsilon}^{nume}$ refer to the exact and numerical solutions of the strains respectively, and A is the area of the problem domain.

5.1. Cantilever subjected to parabolic tractions at the free end

A cantilever is first studied, which is of length L and height D and subjected to a parabolic traction on the right edge, as shown in Fig. 5. The beam is assumed to have unit thickness and the analytical solutions based on the plane stress theory are available as follows [Timoshenko and Goodier (1970)]:

$$u_x = -\frac{py}{6EI} \left[(6L - 3x)x + (2 + \nu) \left(y^2 - \frac{D^2}{4} \right) \right], \quad (45)$$

$$u_y = \frac{p}{6EI} \left[3\nu y^2(L - x) + (4 + 5\nu) \frac{D^2 x}{4} + (3L - x)x^2 \right], \quad (46)$$

$$\sigma_x = -\frac{p(L - x)y}{I}, \quad \sigma_y = 0, \quad \sigma_{xy} = \frac{p}{2I} \left[\frac{D^2}{4} - y^2 \right], \quad (47)$$

where I is the moment of the inertia given as $I = D^3/12$. The values of the parameters are taken as: $E = 3.0 \times 10^7$ Pa, $\nu = 0.3$, $L = 50$ m, $D = 10$ m and $P = -1000$ N.

Using the same set of triangular meshes, as shown in Fig. 6, the cantilever beam is studied using the presented CS-PIM models. Further, this problem is also studied using FEM(T3) or CS-PIM(T2), NS-PIM(T3) and ES-PIM(T3) with the same triangular meshes. The FEM is serving as the “bottom line”: any CS-PIM model that is established based on the smoothed bilinear form is softer than the standard FEM(T3) model which is built based on the standard Galerkin weak form and fully compatible. The NS-PIM is chosen for comparison, because we know it

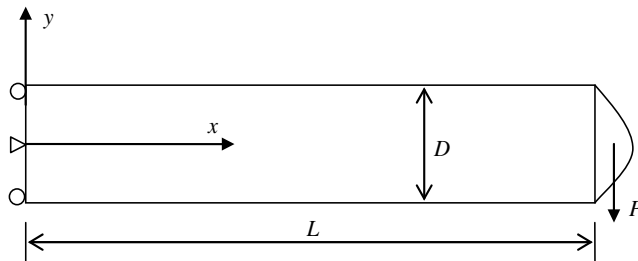


Fig. 5. Cantilever beam subjected to a parabolic traction of the right edge.

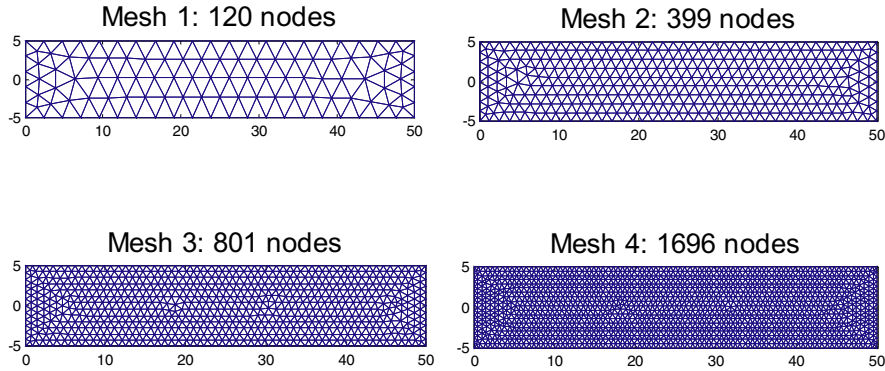


Fig. 6. Domain discretization using three-node triangular cells for the problem of cantilever subjected to a parabolic traction on the right edge.

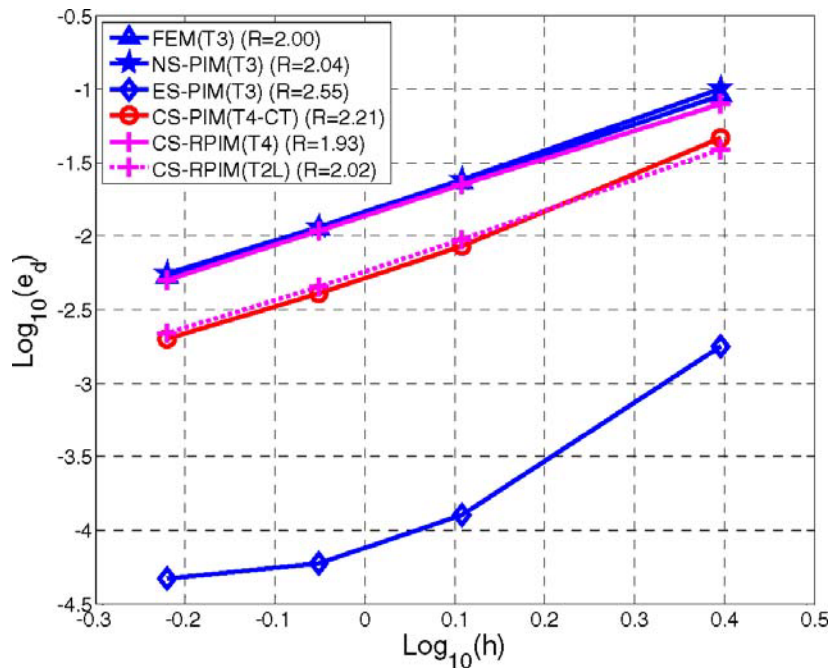


Fig. 7. Convergence of the numerical results in displacement norm for the problem of cantilever solved using different methods and same set of triangular mesh.

gives upper bound solutions [Liu and Zhang (2008a)]. The ES-PIM has been found to have very close-to-exact stiffness and is known as, so far, the most accurate linear model among the numerical methods based on W^2 formulation.

Figure 7 plots the convergence of the solutions in displacement norm for the cantilever solved using different methods. The present CS-RPIM(T4) model, together

with FEM and NS-PIM(T3), converge with the reducing average nodal spacing (h) at about the same rate which is around the theoretical value of 2.0 for both the weak and weakened weak (W^2) formulations [Liu (2008b)]. The CS-PIM(T4-CT) and CS-RPIM(T2L) perform similarly with higher convergence rate and better accuracy than the previous three models. In terms of both convergence and accuracy, the ES-PIM(T3) stands out clearly. Figure 8 plots the convergence of the solutions in energy norm for the cantilever problem solved using different methods. It can be found that CS-RPIM(T4) obtains similar results compared to the FEM and all the other models obtain much higher convergence rate and better accuracy than the FEM. We know that the theoretical convergence rate in energy norm of FEM based on weak form is 1.0 and the ideal rate in energy norm for a W^2 formulation is 1.5 [Liu (2008b)]. For this case, the numerical convergence rate of FEM is found 0.99, which is very close to the theoretical one for weak formulation. The convergence rates of all the methods based on W^2 formulation, except the CS-RPIM(T4), are between 1.0 and 1.5. In terms of both accuracy and convergence rate, the CS-PIM(T4-CT) performs the best among all the methods studied here.

To study the efficiency of these methods, we plotted the errors in displacement and energy norms against the computational cost (seconds), as shown in

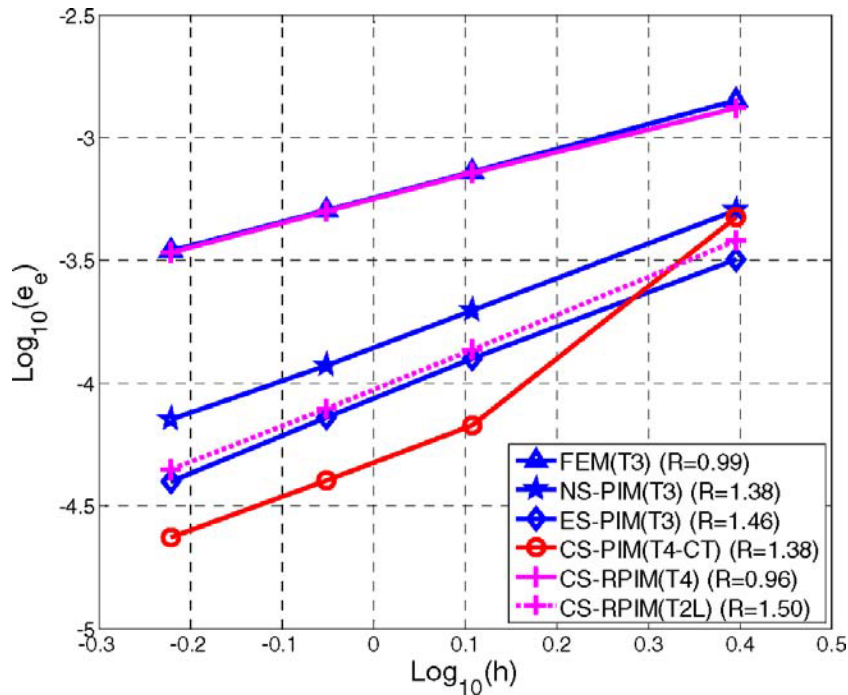


Fig. 8. Convergence of the numerical results in energy norm for the problem of cantilever solved using different methods and same set of triangular mesh.

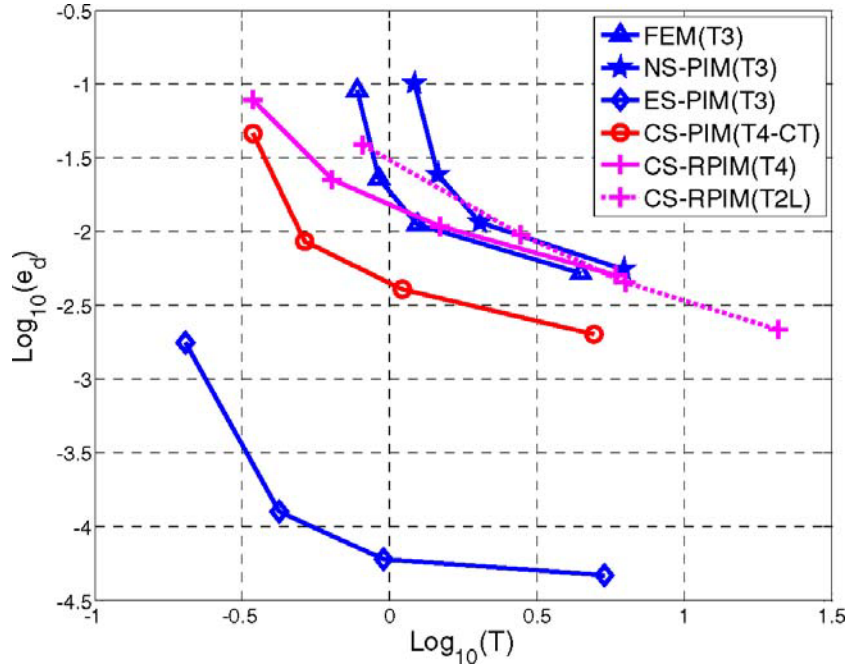


Fig. 9. Computational cost (seconds) versus error in displacement norm. Comparison of efficiency between different methods via the problem of cantilever.

Figs. 9 and 10 respectively. It is found that the CS-RPIM(T4) has similar efficiency compared to the FEM. The CS-RPIM(T2L) and the NS-PIM(T3) have similar efficiency, and they perform better with respect to energy norm error than the previous two methods. Among all the methods, the CS-PIM(T4-CT) and the ES-PIM(T3) perform better than the others and respectively they have the best efficiency with respect to energy and displacement norm errors.

Figure 11 plots the process of strain energies converging to the exact solution for the cantilever using different methods. The exact value of strain energy for this problem is 8.593333333, which is calculated by analytical integration using the stresses given in Eq. (47). As we expected, FEM and NS-PIM give lower and upper bound respectively and also provide the energy bound to other models. The CS-RPIM(T4) has been found has a close stiffness as the FEM and converges to the exact one from below. The CS-PIM(T4-CT) and the CS-RPIM(T2L) have similar stiffness: they are much softer than the FEM and stiffer than the overly-soft NS-PIM. As we discussed previously [Liu and Zhang (2008a)], one issue that effects the softness of the model is the order of shape functions used in the displacement approximation: when higher order shape functions are used, the displacements approximated in a smoothing domain are closer to the exact solution, which will reduce the stiffening effect and vice versa. As the T2L scheme uses more nodes than T4 scheme for

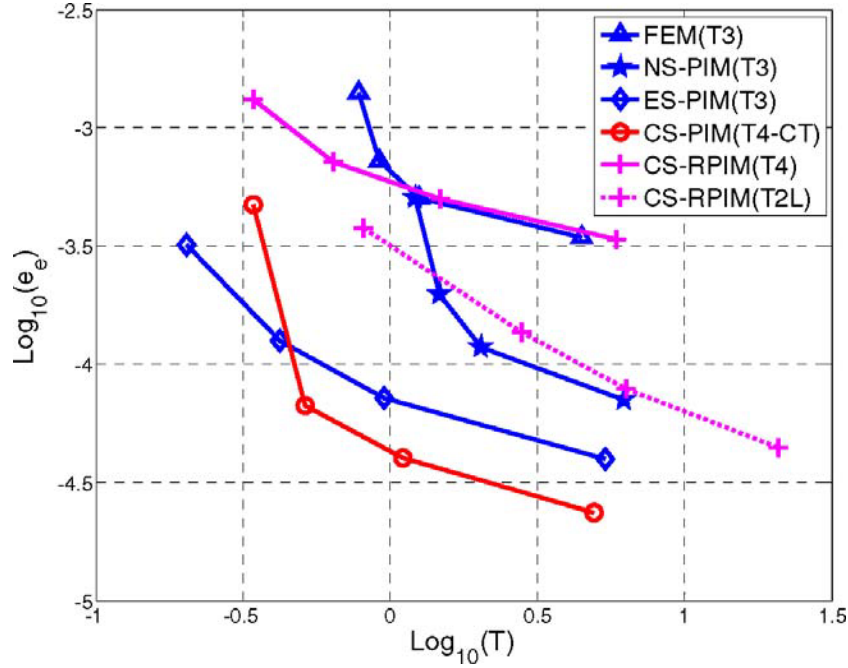


Fig. 10. Computational cost (seconds) versus error in energy norm. Comparison of efficiency between different methods via the problem of cantilever.

interpolation of displacements, thus we can find from Fig. 11 that the CS-RPIM with T2L scheme performs much softer than the CS-RPIM of T4 scheme. For this case, the ES-PIM(T3) has the most close-to-exact stiffness and its solutions are the closest to the exact one. The solutions of CS-PIM(T4-CT) and CS-RPIM(T2L) are in between of those of the NS-PIM(T3) and the ES-PIM (T3).

5.2. Infinite solid with a circular hole

The second benchmark problem is an infinite solid with a central circular hole ($a = 1$) and subjected to a unidirectional tensile ($T_x = 10$), as shown in Fig. 12. Due to the two-fold symmetry, only one quarter is modeled with $b = 5$ and symmetry conditions are imposed on the left and bottom edges. The analytical solution is available for this problem as follows [Timoshenko and Goodier (1970)]:

$$u_x = \frac{T_x a}{8\mu} \left[\frac{r}{a} (\kappa + 1) \cos \theta + 2 \frac{a}{r} ((1 + \kappa) \cos \theta + \cos(3\theta)) - 2 \frac{a^3}{r^3} \cos(3\theta) \right], \quad (48)$$

$$u_y = \frac{T_x a}{8\mu} \left[\frac{r}{a} (\kappa - 3) \sin \theta + 2 \frac{a}{r} ((1 - \kappa) \sin \theta + \sin(3\theta)) - 2 \frac{a^3}{r^3} \sin(3\theta) \right], \quad (49)$$

$$\sigma_{xx} = T_x \left\{ 1 - \frac{a^2}{r^2} \left[\frac{3}{2} \cos(2\theta) + \cos(4\theta) \right] + \frac{3a^4}{2r^4} \cos(4\theta) \right\}, \quad (50)$$

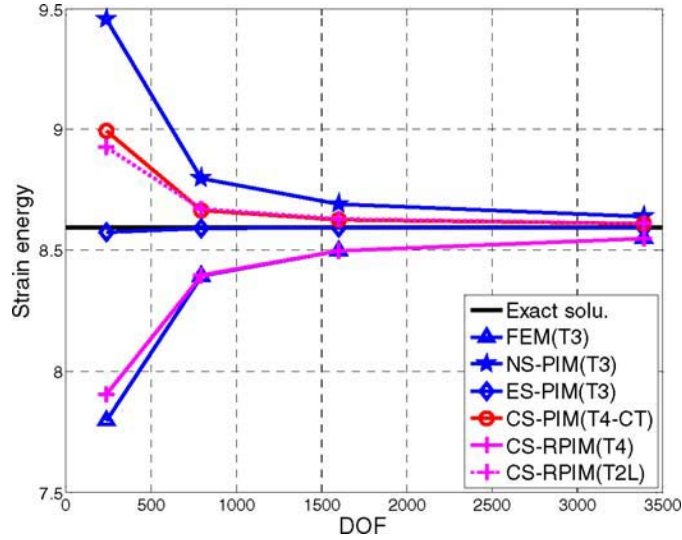


Fig. 11. Solutions (in energy norm) converging to the exact solution for the problem of cantilever obtained using different methods and same set of irregular triangular mesh.

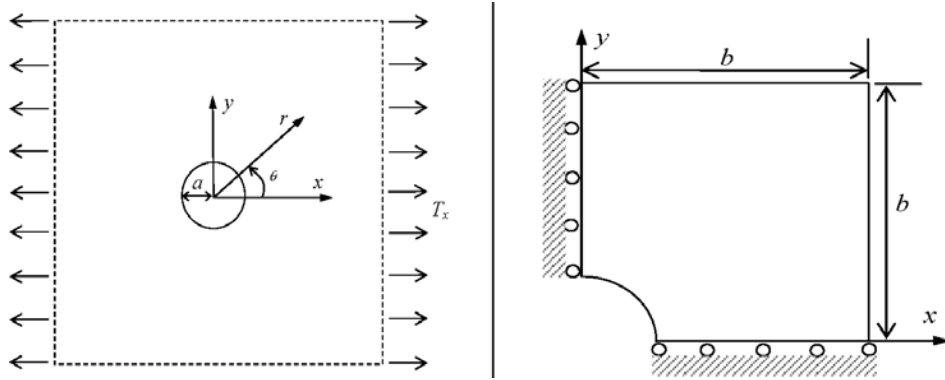


Fig. 12. Infinite solid with a circular hole subjected to uniform tensile and its quadrant model.

$$\sigma_{yy} = -T_x \left\{ \frac{a^2}{r^2} \left[\frac{1}{2} \cos(2\theta) - \cos(4\theta) \right] + \frac{3a^4}{2r^4} \cos(4\theta) \right\}, \quad (51)$$

$$\sigma_{xy} = -T_x \left\{ \frac{a^2}{r^2} \left[\frac{1}{2} \sin(2\theta) + \sin(4\theta) \right] - \frac{3a^4}{2r^4} \sin(4\theta) \right\}, \quad (52)$$

where μ is the shear modulus and κ is the Kolosov which are defined as

$$\mu = \frac{E}{2(1+\nu)} \quad \kappa = \begin{cases} 3-4\nu & \text{Plane strain} \\ \frac{3-\nu}{1+\nu} & \text{Plane stress} \end{cases}. \quad (53)$$

In the above equations, (r, θ) are the polar coordinates and θ is measured counterclockwise from the positive x -axis. We studied the problem under plane stress conditions and traction boundary conditions are imposed on the right and upper edges with the exact stresses obtained using Eqs. (50)–(52).

Using the same set of triangular meshes, shown in Fig. 13, this problem is studied using the present method, together with the standard FEM, NS-PIM(T3) and ES-PIM(T3). The convergence property in terms of displacement of all the methods is shown in Fig. 14. Again we found that the NS-PIM(T3) and CS-RPIM(T4) obtain similar results as FEM. All the other models provide much more accurate and faster convergent solutions than the FEM. In terms of both convergence and accuracy, the CS-PIM(T4-CT), together with the CS-RPIM(T2L), stand out in the displacement norm. Figure 15 shows the convergence property in terms of energy error for all the methods. The CS-RPIM(T4) obtains close results to the standard FEM and performs the worst among the methods based on W^2 formulation. Results of the NS-PIM(T3) and the ES-PIM(T3) have similar performance which are much better than the FEM. We found for this example that the CS-PIM(T4-CT) and the CS-RPIM(T2L) stand out also in the energy norm.

Figure 16 shows the process of strain energies converging to the exact one for the infinite solid problem solved using different methods, in which the exact strain

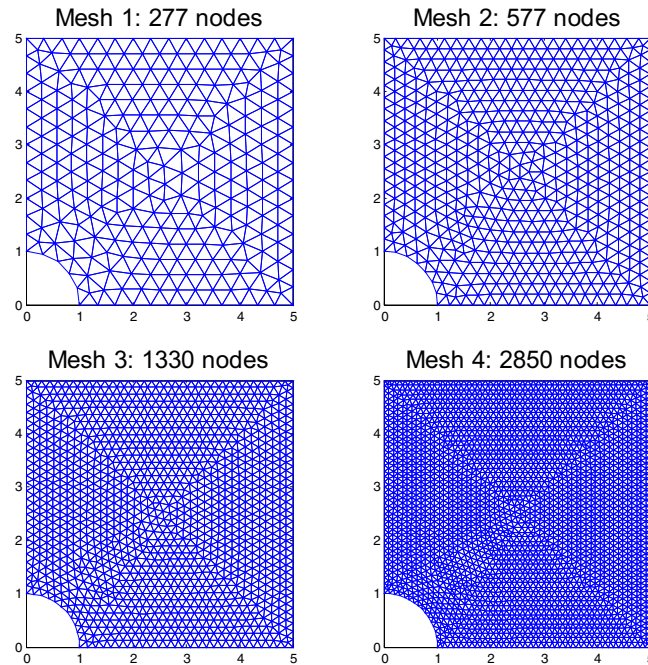


Fig. 13. Domain discretization using three-node triangular cells for the quadrant model of the problem of infinite solid with a circular hole subjected to uniform tensile.

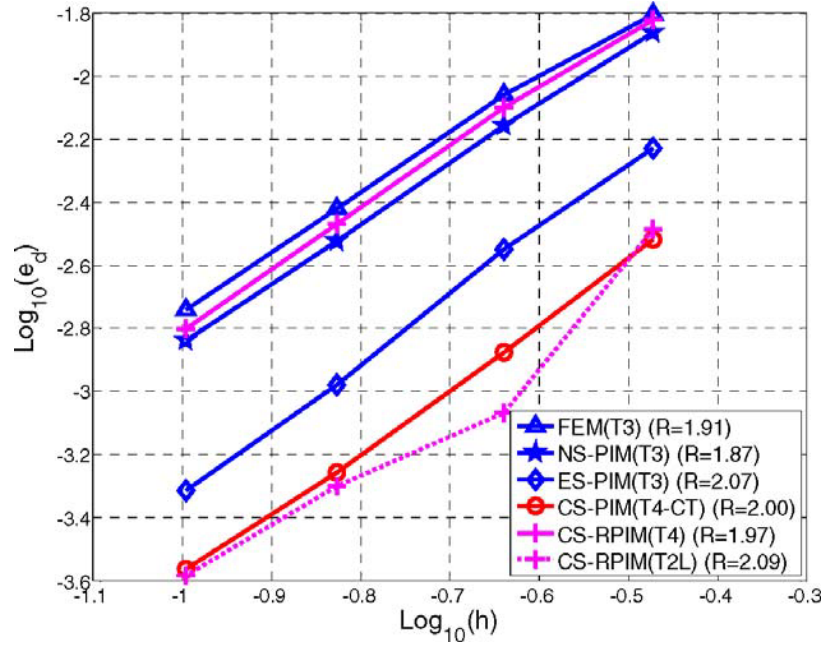


Fig. 14. Convergence of the numerical results in displacement norm for the problem of infinite solid with a hole solved using different methods and same set of irregular triangular mesh.

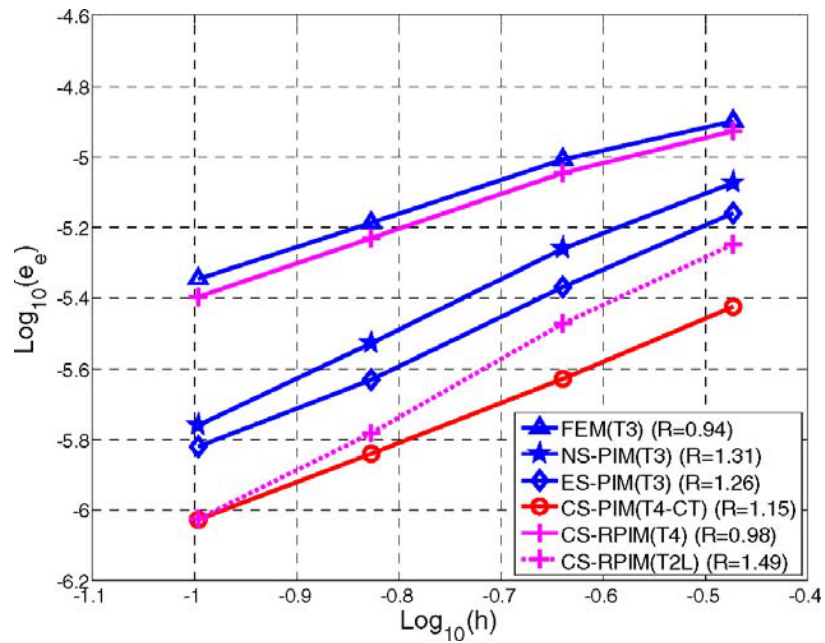


Fig. 15. Convergence of the numerical results in energy norm for the problem of infinite solid with a hole solved using different methods and same set of irregular triangular mesh.

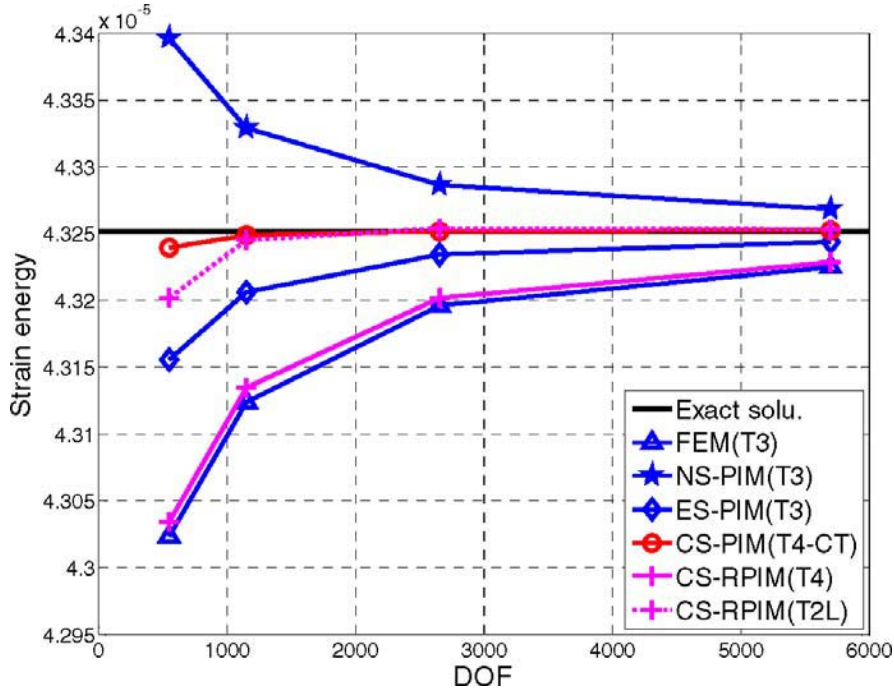


Fig. 16. Solutions (in energy norm) converging to the exact solution for the problem of infinite solid with a hole obtained using different methods and same set of irregular triangular mesh.

energy is calculated using the stresses given in Eqs. (50)–(52) by analytical integration and the value is $4.325139892E-5$. FEM and NS-PIM provide lower and upper bound solutions respectively and they also bound the solutions of other models from two sides. The CS-RPIM(T4) model performs a little softly than the FEM and converges to the exact one from below. The other three models are much softer than the overly-stiff FEM and stiffer than the overly-soft NS-PIM model. Among all the methods, the CS-PIM(T4-CT) and the CS-RPIM(T2L) give the closet solution to the exact one.

5.3. Free vibration of a slender rectangular cantilever

In this example, free vibration analysis is performed for a slender cantilever beam with $L = 100$ mm, $D = 10$ mm, thickness $t = 1.0$ mm, Young's modulus $E = 2.1 \times 10^4$ kgf/mm², Poisson's ratio $\nu = 0.3$, mass density $\rho = 8.0 \times 10^{-10}$ kgf s²/mm⁴. A plane stress problem is considered. Because the slenderness of the beam, the Euler-Bernoulli beam theory is used to obtain the fundamental frequency $f_1 = 0.08276 \times 10^4$ Hz as a reference. Three regular meshes are used in the analysis. Numerical results using the FEM of four node quadrangular elements (FEM-Q4)

Table 2. First twelve natural frequencies (in 10 kHz) of the slender cantilever.

Model	CS-PIM (T4-CT)	CS-RPIM (T4)	CS-RPIM (T2L)	ES-PIM (T3)	FEM (T3)	Reference solu.
Mesh: 10×1	0.0576	0.0701	0.0675	0.1048	0.1692	0.0824
Nodes: 22	0.3440	0.4190	0.4003	0.6018	0.9163	0.4944
Background cells:	0.9057	1.0922	1.0210	1.2833	1.2869	1.2824
Three-node triangular cell	1.2803	1.2818	1.2826	1.5177	2.1843	1.3022
	1.6471	1.9525	1.7454	2.6362	3.5942	2.3663
	2.4993	2.8935	2.4536	3.7724	3.8338	3.6085
	3.3973	3.7638	3.1601	3.8559	5.0335	3.8442
	3.7957	3.8859	3.7864	5.0349	6.2421	4.9674
	4.2743	4.6550	3.9648	6.0827	6.4154	6.3960
	4.8330	4.9178	4.8932	6.1520	7.5940	6.4023
	4.9122	5.1483	5.6160	7.0519	8.4790	7.8853
	5.1088	5.2525	5.8589	7.7212	8.7033	8.9290
Mesh: 20×2	0.0769	0.0804	0.0754	0.0853	0.1117	0.0824
Nodes: 63	0.4623	0.4833	0.4578	0.5078	0.6539	0.4944
Background cells:	1.2227	1.2772	1.2266	1.2828	1.2843	1.2824
Three-node triangular cell	1.2823	1.2841	1.2827	1.3246	1.6748	1.3022
	2.2325	2.3360	2.2734	2.3783	2.9554	2.3663
	3.4165	3.5774	3.5298	3.5784	3.8424	3.6085
	3.8350	3.8411	3.8353	3.8298	4.3866	3.8442
	4.7133	4.9426	4.9287	4.8533	5.8836	4.9674
	6.0720	6.3374	6.3429	6.1527	6.3751	6.3960
	6.3512	6.4129	6.4111	6.3182	7.4046	6.4023
	7.4630	7.8432	7.9040	7.4419	8.8210	7.8853
	8.7693	8.8507	8.7874	8.6776	8.9411	8.9290
Mesh: 40×4	0.0809	0.0819	0.0805	0.0827	0.0906	0.0824
Nodes: 205	0.4858	0.4918	0.4825	0.4950	0.5409	0.4944
Background cells:	1.2810	1.2825	1.2699	1.2826	1.2831	1.2824
Three-node triangular cell	1.2825	1.2978	1.2825	1.3006	1.4161	1.3022
	2.3308	2.3631	2.3054	2.3554	2.5570	2.3663
	3.5572	3.6107	3.5112	3.5778	3.8433	3.6085
	3.8421	3.8437	3.8436	3.8408	3.8786	3.8442
	4.8981	4.9791	4.8258	4.9029	5.3087	4.9674
	6.3102	6.3896	6.2071	6.2867	6.3935	6.3960
	6.3862	6.4283	6.3922	6.3774	6.8093	6.4023
	7.7646	7.9212	7.6261	7.6987	8.3473	7.8853
	8.8996	8.9164	8.9177	8.8751	8.9183	8.9290

with a very fine mesh (100×10) for the same problem are computed and used as reference solutions.

Table 2 lists the first twelve natural frequencies of the cantilever solved using different methods. The first twelve vibration modes obtained using the CS-PIM(T4-CT) and CS-RPIM(T2L) are plotted in (a) and (b) of Fig. 17, respectively. No spurious modes have been found for the present method. The natural frequencies obtained using the present CS-PIM models are smaller than those of FEM, especially when less background cells are used, which also explains that the present method performs more softly than the FEM.

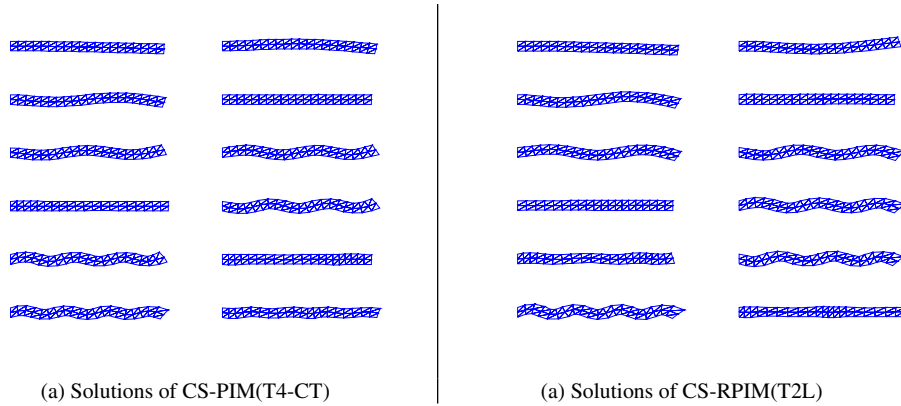


Fig. 17. First 12 free vibration modes of the slender cantilever by the CS-PIM models.

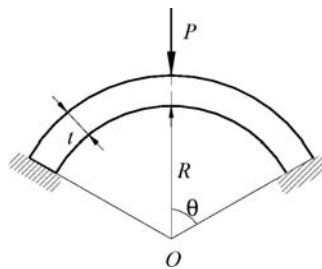


Fig. 18. A spherical shell subjected to point loading at the apex.

5.4. Forced vibration analysis of a spherical shell

Finally, a forced vibration analysis is conducted for the spherical shell shown in Fig. 18. The shell is subjected to a concentrated loading at its apex, and is modeled as 2D plane strain problem. A half of the shell is modeled using triangular meshes. The non-dimensional parameters used in the computation are $R = 12$, $t = 0.1$, $\phi = 10.9^\circ$, $\theta = 0.5$, $E = 1.0$, $\nu = 0.3$, and $\rho = 1.0$.

This problem is first studied by subjected to a harmonic loading of $f(t) = \cos \omega_f t$, and the time history of the deflection at the apex of the shell is plotted in Fig. 19 with $\omega_f = 0.05$ and $\Delta t = 5$. It is found that the solution of the CS-PIM(T4-CT) is very close to that of the ES-PIM(T3), whose results have been found comparable to those obtained using the eight-nodes quadrilateral elements of FEM [Liu Nguyen and Lam (2008)]. For this case, the amplitude of the CS-RPIM(T2L) results is a litter bigger than that of the CS-PIM(T4-CT). Thus the present two CS-PIM models can obtain much more accurate results than the linear FEM. Then the shell excited by a constant step load $f(t) = 1$ starting from $t = 0$ is studied using the CS-PIM(T4-CT) and the response is plotted in Fig. 20. The

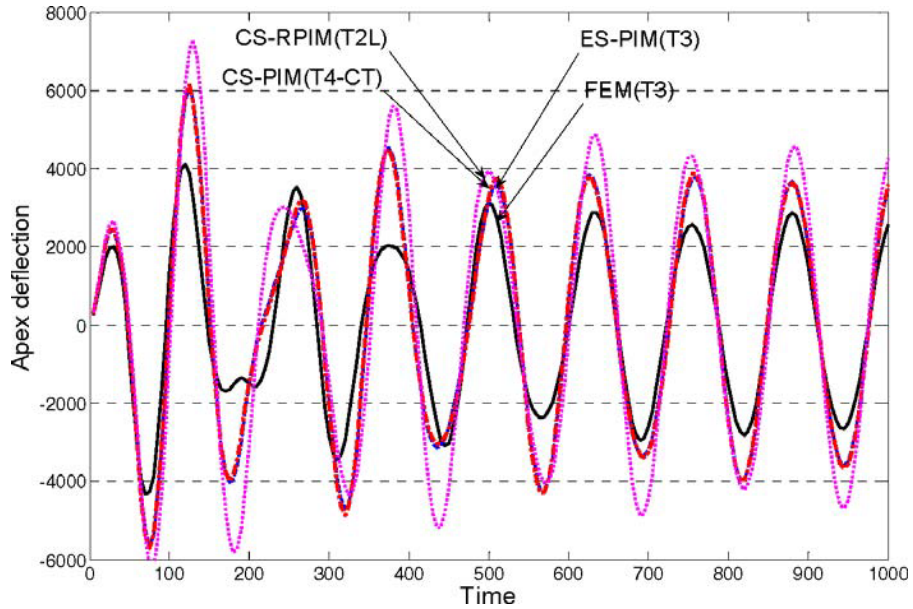


Fig. 19. Solutions of transient responses of the spherical shell subjected to a harmonic loading using different methods.

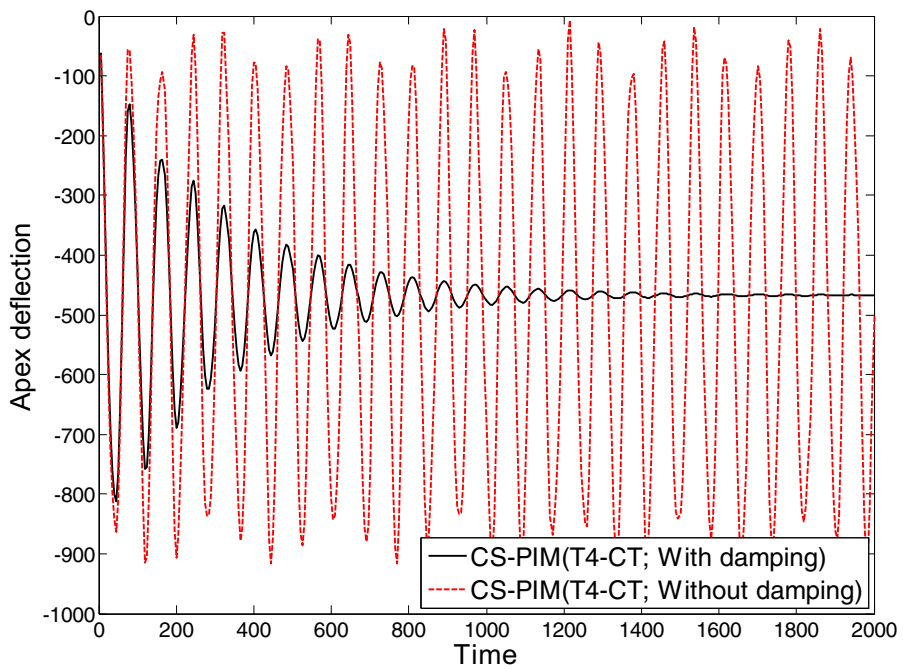


Fig. 20. Solutions of transient responses of the spherical shell subjected to a constant step loading using the CS-PIM(T4-CT).

dash line is for the results without damping, and we found that the amplitude of the deflection tends to a constant value with increasing time. When a Rayleigh damping of $\alpha = 0.005$ and $\beta = 0.272$ are considered, the response converges to constant very quickly.

6. Conclusions

In this work, a normed G^1 space and a weakened weak (W^2) formulation for solid mechanics problems have been first briefly presented. Using the W^2 formulation, a cell-based smoothed point interpolation method (CS-PIM) has been proposed, in which the displacement fields are approximated using PIM shape functions (polynomial PIM or radial PIM) and the generalized smoothed strains are obtained over each triangular background cells. A set of edge-based T-schemes for nodes selection of interpolation have been proposed and an adaptive coordinate transformation (CT) has been presented to solve the singularity problem encountered in constructing bilinear polynomial PIM shape functions. According to different PIM shape functions and T-schemes used, three CS-PIM models have been developed. i.e. CS-PIM(T4-CT), CS-RPIM(T4) and CS-RPIM(T2L). A number of numerical example problems, including static, free and forced vibration analysis, have been studied to investigate the properties of those CS-PIM models. Through these investigations, the following conclusions can be drawn.

- Without introducing additional degrees of freedom, the present method is very easy to implement and works well using the simplest linear triangular mesh.
- All the three CS-PIM models can pass the standard patch test and thus they are at least linearly conforming.
- The coordinates transformation (CT) technique can successfully resolve the singularity problem encountered in the process of constructing bilinear polynomial PIM shape functions.
- The CS-PIM(T4-CT) stands out from all the methods studied in this work. Compared to other methods, it shows higher convergence rate and efficiency, better accuracy, and more close-to-exact stiffness for the static analysis. Furthermore, it is temporally stable and works well for dynamic analysis.
- The CS-RPIM(T4) model performs a little softer than the linear FEM and has the feature of overly-stiff. Thus the results of it are a little better than that of the FEM but much worse than other methods based on W^2 formulation. Also, the CS-RPIM(T4) model is temporally stable.
- The CS-RPIM(T2L) shows similar convergence rate, accuracy and stiffness as the CS-PIM(T4-CT). Due to more nodes selected for the construction of RPIM shape functions, it is more expensive than the others and hence has lower efficiency. This model is also temporally stable. The CS-RPIM(T2L) can perform very well for thin plates [Cui and Liu *et al.* (2009)].

References

- Chen, J. S., Wu, C. T. and Belytschko, T. [2000] Regularization of material instabilities by meshfree approximations with intrinsic length scales, *International Journal for Numerical Methods in Engineering* **47**, 1303–1322.
- Chen, J. S., Wu, C. T., Yoon, S. and You, Y. [2001] A stabilized conforming nodal integration for Galerkin mesh-free methods, *International Journal for Numerical Methods in Engineering* **50** 435–466.
- Cui, X. Y., Liu, G. R., Li, G. Y. and Zhang, G. Y. [2009] A thin plate formulation without rotation DOFs based on the radial point interpolation method and triangular cells, *International Journal for Numerical Methods in Engineering*, submitted.
- Dai, K. Y., Liu, G. R. and Nguyen, T. T. [2007] An n-sided polygonal smoothed finite element method (nSFEM) for solid mechanics, *Finite Elements in Analysis and Design* **43**, 847–860.
- Dai, K. Y. and Liu, G. R. [2007] Free and forced analysis using the smoothed finite element method (SFEM), *Journal of Sound and Vibration* **301**, 803–820.
- Eringen, A. C. and Edelen, D. G. B. [1972] On nonlocal elasticity, *Int. J. Eng. Sci.* **10**, 233–248.
- Liu, G. R. [2002] *Meshfree Methods: Moving Beyond the Finite Element Method* (CRC Press, Boca Raton, USA).
- Liu, G. R. [2008a] A generalized gradient smoothing technique and the smoothed bilinear form for Galerkin formulation of a wide class of computational methods, *International Journal of Computational Methods* **5**(2), 199–236.
- Liu, G. R. [2008b] A weakened weak (W^2) form for a unified formulation of compatible and incompatible methods, Part I: Theory and Part II: Applications to solid mechanics problems, *International Journal for Numerical Methods in Engineering* (revised).
- Liu, G. R., Dai, K. Y. and Nguyen, T. T. [2007] A smoothed finite element method for mechanics problems, *Computational Mechanics* **39**, 859–877.
- Liu, G. R. and Gu, Y. T. [2001] A point interpolation method for two-dimensional solids, *International Journal for Numerical Methods in Engineering* **50**, 937–951.
- Liu, G. R. and Gu, Y. T. [2005] *An Introduction to Meshfree Methods and Their Programming* (Springer, Dordrecht, The Netherlands).
- Liu, G. R. and Liu, M. B. [2003] *Smoothed Particle Hydrodynamics — A Meshfree Particle Method* (World Scientific, Singapore).
- Liu, G. R. and Quek, S. S. [2003] *Finite Element Method: A Practical Course* (Butterworth-Heinemann, Burlington, MA).
- Liu, G. R. and Zhang, G. Y. [2008a] Upper bound solution to elasticity problems: A unique property of the linearly conforming point interpolation method (LC-PIM), *International Journal for Numerical Methods in Engineering* **74**, 1128–1161.
- Liu, G. R. and Zhang, G. Y. [2008b] Edge-based smoothed point interpolation methods, *International Journal of Computational Methods* **5**(4), 621–646.
- Liu, G. R. and Zhang, G. Y. [2008c] A strain-constructed point interpolation method (SC-PIM) and strain field construction schemes for mechanics problems of solids and structures using triangular mesh, *International Journal of Solids and Structures* (submitted).
- Liu, G. R., Nguyen, T. T., Dai, K. Y. and Lam, K. Y. [2007] Theoretical aspects of the smoothed finite element method (SFEM), *International Journal for Numerical Methods in Engineering* **71**, 902–930.
- Liu, G. R., Nguyen, T. T. and Lam, K. Y. [2008]. An edge-based smoothed finite element method (ES-FEM) for static and dynamic problems of solid mechanics, *Journal of Sound and Vibration*, published on line, doi:10.1016/j.jsv.2008.08.027.

- Liu, G. R., Nguyen, T. T., Nguyen, X. H. and Lam, K. Y. [2008] A node-based smoothed finite element method (NS-FEM) for upper bound solutions to solid mechanics problems, *Computers and Structures*, published on line, doi:10.1016/j.compstruc.2008.09.003.
- Liu, G. R., Xu, X., Zhang, G. Y. and Gu, Y. T. [2009a] An extended Galerkin weak form and a point interpolation method with continuous strain field and superconvergence using triangular mesh, *Computational Mechanics* **43**, 651–673.
- Liu, G. R., Xu, X., Zhang, G. Y. and Nguyen, T. T. [2009b] A superconvergence point interpolation method (SC-PIM) with piecewise linear strain field using triangular mesh, *International Journal for Numerical Methods in Engineering* **77**, 1439–1467.
- Liu, G. R., Zhang, G. Y., Dai, K. Y., Wang, Y. Y., Zhong, Z. H., Li, G. Y. and Han, X. [2005] A linearly conforming point interpolation method (LC-PIM) for 2D mechanics problems, *International Journal of Computational Methods* **2**(4), 645–665.
- Liu, G. R., Li, Y., Dai, K. Y., Luan, M. T. and Xue, W. [2006] A linearly conforming radial point interpolation method for solid mechanics problems, *International Journal of Computational Methods* **3**, 401–428.
- Lucy, L. B. [1977], Numerical approach to testing the fission hypothesis, *Astronomical Journal* **82**, 1013–1024.
- Monaghan, J. J. [1982] Why particle methods work (hydrodynamics), *SIAM Journal on Scientific and Statistical Computing* **3**, 422–433.
- Nguyen, T. T., Liu, G. R., Lam, K. Y. and Zhang, G. Y. [2008] A Face-based Smoothed Finite Element Method (FS-FEM) for 3D linear and nonlinear solid mechanics problems using 4-node tetrahedral elements, *International Journal for Numerical Methods in Engineering*, published on line, doi: 10.1002/nme.2491.
- Pian, T. H. H. and Wu, C. C. [2006] *Hybrid and Incompatible Finite Element Methods* (CRC Press, Boca Raton).
- Powell, M. J. D. [1992]. The theory of radial basis function approximation in 1990, in *Advances in Numerical Analysis*, ed. Light, F. W. (Oxford University Press, Oxford), pp. 303–322.
- Timoshenko, S. P. and Goodier, J. N. [1970] *Theory of Elasticity*, 3rd edn. (McGraw-Hill, New York).
- Wang, J. G. and Liu, G. R. [2002] A point interpolation meshless method based on radial basis functions, *International Journal for Numerical Methods in Engineering* **54**, 1623–1648.
- Zhang, G. Y., Liu, G. R. and Li, Y. [2008] An efficient adaptive analysis procedure for certified solutions with exact bounds of strain energy for elasticity problems, *Finite Elements in Analysis and Design* **44**, 831–841.
- Zhang, G. Y., Liu, G. R., Nguyen, T. T., Song, C. X., Han, X., Zhong, Z. H. and Li, G. Y. [2007a] The upper bound property for solid mechanics of the linearly conforming radial point interpolation method (LC-RPIM), *International Journal of Computational Methods* **4**(3), 521–541.
- Zhang, G. Y., Liu, G. R., Wang, Y. Y., Huang, H. T., Zhong, Z. H., Li, G. Y. and Han, X. [2007b] A linearly conforming point interpolation method (LC-PIM) for three-dimensional elasticity problems, *International Journal for Numerical Methods in Engineering* **72**, 1524–1543.
- Zienkiewicz, O. C. and Taylor, R. L. [2000] *The Finite Element Method* 5th edn. (Butterworth Heinemann, Oxford, UK).

